Projecting Lane Lines from Proxy High-Definition Maps for Automated Vehicle Perception in Road Occlusion Scenarios

Author, co-author (Do NOT enter this information. It will be pulled from participant tab in MyTechZone)

Affiliation (Do NOT enter this information. It will be pulled from participant tab in MyTechZone)

Abstract

Contemporary ADS and ADAS localization technology utilizes real-time perception sensors such as visible light cameras, radar sensors, and lidar sensors, greatly improving transportation safety in sufficiently clear environmental conditions. However, when lane lines are completely occluded, the reliability of on-board automated perception systems breaks down, and vehicle control must be returned to the human driver. This limits the operational design domain of automated vehicles significantly, as occlusion can be caused by shadows, leaves, or snow, which all occur in many regions. High-definition map data, which contains a high level of detail about road features, is an alternative source of the required lane line information. This study details a novel method where high-definition map data are processed to locate fully occluded lane lines, allowing for automated path planning in scenarios where it would otherwise be impossible. A proxy high-definition map dataset with high-accuracy lane line geospatial positions was generated for routes at both the Eaton Proving Grounds and Campus Drive at Western Michigan University (WMU). Once map data was collected for both routes, the WMU Energy Efficient and Autonomous Vehicles Laboratory research vehicles were used to collect video and high-accuracy GNSS data. The map data and GNSS data were fused together using a sequence of data processing and transformation techniques to provide occluded lane line geometry from the perspective of the ego vehicle camera system. The recovered geometry is then overlaid on the video feed to provide lane lines, even when they are completely occluded and invisible to the camera. This enables the control system to utilize the projected lane lines for path planning, rather than failing due to undetected, occluded lane lines. This initial study shows that utilization of technology outside of the norms of automated vehicle perception successfully expands the operational design domain to include occluded lane lines, a necessary and critical step for the achievement of complete vehicle autonomy.

Introduction

The US Centers for Disease Control and Prevention (CDC) and the US National Highway Traffic Safety Administration (NHTSA) report that motor vehicle accidents account for nearly 40,000 US deaths in 2019 and comprised the 13th leading cause of death in the US in 2016 and 2017 [1-3]. CDC data indicates the estimated cost of US motor vehicle fatalities to be about $390 billion in 2019 when accounting for both medical costs and economic productivity losses [4]. Additionally, motor vehicle traffic crashes consistently rank the 7th greatest contributor to years of life lost, as they disproportionately cause more deaths to younger people [3]. In response to the great cost of motor vehicle accidents, the emerging technological field of vehicle automation seeks to mitigate motor vehicle accidents and injuries. While in the future, high levels of autonomy through Automated Driving Systems (ADS) and Autonomous Vehicles (AVs) will be available, some vehicles available today offer Advanced Driver Assistance Systems (ADAS) features to improve safety.

ADAS features such as lane departure warning (LDW), lane keeping assistance (LKA), and lane centering assistance (LCA) can dramatically improve motor vehicle safety. LDW reduces single-vehicle, sideswipe, and head-on injury crashes by 21% [5]. It is estimated by Benson et al. that LDW and LKA could have prevented about 520,000 crashes in 2016, associated with about 190,000 injuries. They also report that ADAS technology at large has the potential to mitigate 40% of all passenger vehicle crashes, and about 30% of all crash-related deaths [6]. In terms of the cost of motor vehicle accidents, Harper, Hendrickson, and Samaras estimate that incorporating ADAS features into the entire US light-duty vehicle fleet would lead to an annual net savings of between $4 billion to $215 billion when considering the cost of the technology and the cost of motor vehicle crash injuries and deaths [7]. ADAS has also been demonstrated to be useful for enabling energy efficiency improvements for individual vehicles [8-11]. But, these ADAS features have an operational design domain (ODD) limited to unoccluded lane lines, as they work by using real-time perceptive sensors such as computer vision (CV) to detect road features, primarily lane lines, which are normally visible in clear driving environments [12-14]. However, many vehicle crashes occur in inclement weather, where road features can be completely occluded by snow or ice.

In fact, while vehicles regularly travel less in winter seasons as evidenced by seasonal vehicle-miles-traveled trends, the inclement driving environment conditions associated with the colder seasons leads to increased vehicle accidents and fatalities [15-16], as seen in Figure 1. According to the Federal Highway Administration

(FHWA), approximately 21% of all vehicle crashes in the US from 2007 to 2016 were weather-related [17]. The ODD of vehicle autonomy does not effectively include inclement weather conditions where lane lines are occluded, as perception systems lack the necessary input to determine road geometry [18-19]. It is estimated that approximately 70% of US roads are located in snowy regions, meaning for higher levels of automation throughout the continental US, the ODD of automated vehicles must be expanded to handle roads occluded by snow and ice [20].

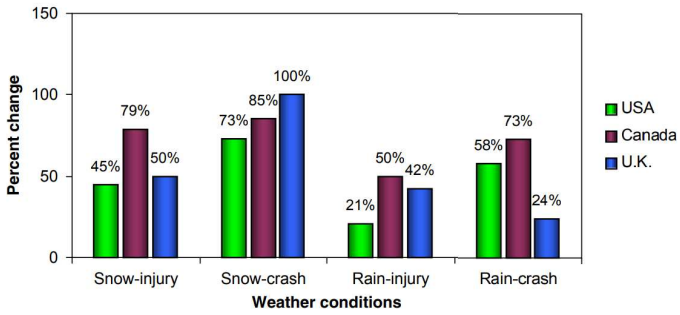

Figure 1. Percent changes in crash rate due to inclement weather [16].

Greater connectivity of the vehicle to the internet of things has great potential to aid automated vehicle technologies [21]. Specifically, the utilization of high-definition maps for localization of the ego vehicle has been shown to have great potential. High-definition maps are datasets that contain highly detailed regional data, far surpassing the minimum level of detail required for road network route planning as is available in standard maps. Notably, they can include the positions of road features such as traffic signs, road shape, and lane lines [22]. Little research has focused on occluded lane line scenarios, despite the potential for safety improvements. Poggenhans, Salscheider, and Stiller present a method of localization where high-definition maps are queried with estimated lane line locations to determine the true ego vehicle position. This method begins to lose accuracy in inclement weather and relies on real-time perception of road markings, thus would likely break down when lane lines are occluded, similar to the current state-of-the-art [23]. VSI Labs described use of high-definition maps in their study, where lane lines were used directly as an input to the ego vehicle control system, but their exact methodology appears to be proprietary and confidential [24]. High-definition maps have the potential to increase the level of automation of ADS technology, but no method exists with sufficient ability to operate in occluded lane line scenarios. In this paper we describe a novel method for utilizing high-definition map data to expand the ODD of ADS and ADAS technologies to occluded lane line scenarios.

Methods

Data Collection

Though high-definition maps often include lane line geometry, to avoid the cost of a high-definition map service for this study, data was collected manually over two distinct routes in order to generate a proxy high-definition map. The collection of this data is detailed to give more context for the results and to inform those who wish to replicate this study without purchasing a high-definition map service subscription. The first route was selected to be a portion of the Eaton Proving Grounds main test track in Marshall, Michigan, shown in Figure 3. This route contained a straight section, followed by a curve to the left surrounded by trees. The second route was selected to be the Campus Drive loop near Western Michigan University's Parkview Campus, shown in Figure 4. This route consisted of a winding, continuously curving road segment. Several hundred extremely high-precision geospatial points were collected along the right and left lane lines for each route using a Trimble Catalyst DA2 GNSS receiver, as shown in Figure 2, which advertises an accuracy of 2 centimeters when using the Catalyst 1 subscription level. High accuracy geospatial data was especially important in this study, as the lane lines are relatively small and any substantial displacement degrades the results significantly. The distance between collected points was varied, with the Eaton Proving Grounds data being regularly sampled every 50 feet, and the Campus Drive data being sampled about every 10 feet. These both proved to be a small enough sampling distance to sufficiently describe gently curving roads, so it is likely that larger sampling distances would perform reasonably well.

Figure 2. Trimble Catalyst DA2 GNSS receiver [25].

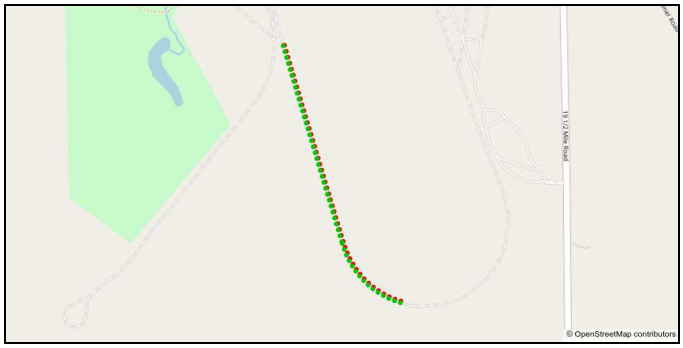

Figure 3. Collected lane line points at the Eaton Proving Grounds test track.

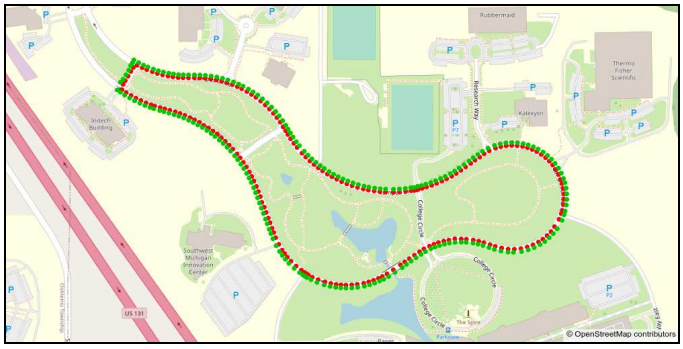

Figure 4. Collected lane line points over the Campus Drive loop.

To achieve smoothed lane lines over both routes, all lane lines points were put in order along the route and cubically interpolated, resulting in many equidistant geospatial points. This interpolation of geospatial points should theoretically be mapped to true distances before interpolation, as the length of latitude and longitude increments is not constant over Earth, but at this relatively small scale the error is negligible. After this step, the proxy high-definition maps for both routes were complete.

The Western Michigan University (WMU) Energy Efficient and Autonomous Vehicles Laboratory research vehicles, shown in Figure 5, were then used to collect data over both routes. The Kia Niro

Hybrid was used at the Eaton Proving Grounds, and the Kia Soul Electric Vehicle was used to collect data over the Campus Drive route. Both vehicles were equipped with the same sensor suite, including but not limited to a Stereolabs ZED 2i stereo camera (Figure 6) and a Swift Navigation Duro Inertial RTK GNSS receiver (Figure 7), which advertises 4 centimeter accuracy when using the Skylark Precise Positioning service.

Figure 5. WMU EEAV Lab research vehicles.

Figure 6. Stereolabs ZED 2i stereo camera [26].

Figure 7. Swift Navigation Duro Inertial RTK GNSS receiver [27].

The ego vehicles were driven over the selected routes and data was collected from the camera, IMU, and GNSS receiver using the Robot Operating System (ROS). The ego vehicle was operated by a human driver, driving no more than 25 miles per hour. A data processing methodology was developed to project lane lines over the camera feed utilizing the sensor data in various ways.

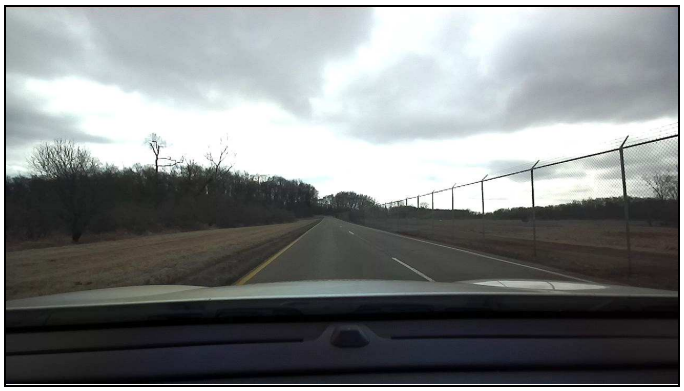

Figure 8. Frame from image data collected over the Eaton Proving Grounds test track.

Figure 9. Frame from image data collected over the Campus Drive loop.

Data Processing

The overarching goal of data processing was to transform the geospatial points of both the lane lines and the ego vehicles into a local coordinate frame aligned with the camera, where the data could be overlaid and given to camera-based path planning systems. To do this, several coordinate transformations were necessary. All points were transformed from the WGS 1984 coordinate system to the north, east, down (NED) coordinate system, with the origin specified as the ego vehicle GNSS base station. This transformation brings the data from a *global* coordinate system into a right-handed *local* coordinate system. The NED coordinate system was chosen over the east, north, up (ENU) coordinate system in order to best match the coordinate system of the camera, shown in Figure 10, as well as the pinhole camera model coordinate system used by the OpenCV Python/C++ library. The coordinate transformation of the lane line points to the NED system was handled by the pymap3d Python library.

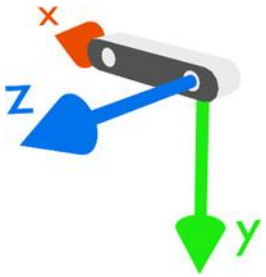

Figure 10. Stereolabs ZED camera coordinate frame [28].

Next, the local NED coordinate frame needed to be rotated to align with the ego vehicle heading. However, the sampling rate of the vehicle heading was insufficient for real-time alignment of the lane line points, especially for curved road segments. To better align with the vehicle over time, IMU data were then used to interpolate the vehicle heading. Measurements of the angular velocity were multiplied by elapsed time to provide angular adjustments to the heading as shown in Equation 1. In summary, the coordinate frame was rotated by the adjusted heading θ about the down axis. This can be represented as shown in Equation 2, where the x-axis is right, the y-axis is down, and the z-axis is forward. This rotation is shown graphically in Figure 11.

$$\theta = \theta_0 - \dot{\theta}\Delta t \tag{1}$$

where:

- θ_0 is the heading reported by the sensor,
- $\dot{\theta}$ is the angular velocity about the IMU (up) z-axis,
- Δt is the time elapsed from the heading sample, and
- θ is the adjusted heading

$$\begin{bmatrix} X_c \\ Y_c \\ Z_c \end{bmatrix} = \begin{bmatrix} -\sin\theta & \cos\theta & 0 \\ 0 & 0 & 1 \\ \cos\theta & \sin\theta & 0 \end{bmatrix} \begin{bmatrix} N \\ E \\ D \end{bmatrix} \quad (2)$$

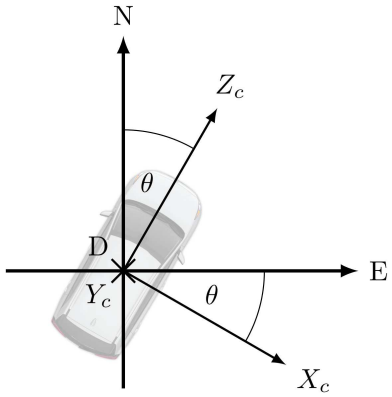

Figure 11. NED to XYZ coordinate frame rotation.

Once all points were rotated to the new XYZ coordinate system, offsets in each direction were used as appropriate to translate from the base station GNSS receiver to the left camera. Once this was complete, all lane line points had been transformed from the global WGS 1984 coordinate system to the local XYZ coordinate system used by the camera. Next, the points needed to be projected onto the camera image feed, applying a maximum-distance threshold if desired. To do this, the pixel location (u, v) of each point must be found, which can be done given the XYZ coordinates and intrinsic camera properties retrieved from the camera metadata. The point projection method equations below are summarized from the OpenCV documentation, following the notation in Figure 12 [29].

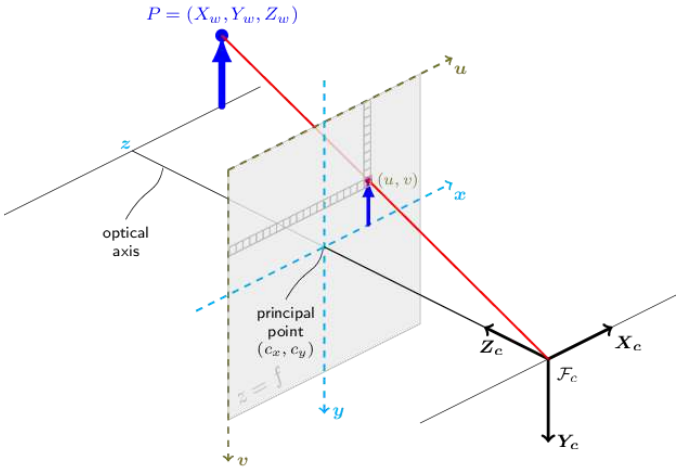

Figure 12. OpenCV pinhole camera model coordinate frame [29].

First, the ratios of the x- and y-coordinates to the z-coordinate of the point are calculated, and the hypotenuse of the x- and y-coordinates r is found.

$$\begin{bmatrix} x' \\ y' \end{bmatrix} = \begin{bmatrix} X_c/Z_c \\ Y_c/Z_c \end{bmatrix} \quad (3)$$

$$r^2 = x'^2 + y'^2 \quad (4)$$

The relevant camera properties were the radial distortion coefficients k_1, k_2, and k_3, the tangential distortion coefficients p_1 and p_2, the principal point coordinates c_x and c_y, and the focal lengths f_x and f_y. These properties can be used to find an intermediate result in both the x- and y-directions. The additional radial distortion coefficients k_4, k_5, and k_6 and thin prism distortion coefficients s_1, s_2, s_3, and s_4 were not necessary and are excluded here.

$$\begin{bmatrix} x'' \\ y'' \end{bmatrix} = \begin{bmatrix} x'(1 + k_1 r^2 + k_2 r^4 + k_3 r^6) + 2p_1 x' y' + p_2(r^2 + 2x'^2) \\ y'(1 + k_1 r^2 + k_2 r^4 + k_3 r^6) + p_1(r^2 + 2y'^2) + 2p_2 x' y' \end{bmatrix} \quad (5)$$

Finally, the projected pixel location (u, v) of the point is found using the focal lengths f_x and f_y and the principal point x- and y-coordinates c_x and c_y.

$$\begin{bmatrix} u \\ v \end{bmatrix} = \begin{bmatrix} f_x x'' + c_x \\ f_y y'' + c_y \end{bmatrix} \quad (6)$$

Sequential application of Equation 3 through Equation 6 results in the appropriate pixel locations of all 3-dimensional points projected onto the 2-dimensional camera image. This is the basis for augmentation of a camera-frame path planning algorithm with high-definition map lane line geometry, without the need for line-of-sight to the lane line.

Additionally, for a sense of distance, a radius or diameter r_{point} for each point to be drawn can be calculated by dividing a size scaling factor s by the distance of the point from the origin, and rounding the result to the nearest integer. This is shown in Equation 7 and Equation 8. Alternatively, as shown in this study, a polygonal chain can be drawn connecting all points for a result that most closely imitates lane lines.

$$dist = \sqrt{X_c^2 + Y_c^2 + Z_c^2} \quad (7)$$

$$r_{point} = \text{round}(s/dist) \quad (8)$$

Artificial Occlusion of Lane Lines

For result comparison, lane lines were extracted from the data using CV techniques. Hue/saturation/lightness thresholding masks were created to isolate yellow and white lane line pixels. While this did successfully identify the appropriate pixels, many pixels from the sky and background passed through the threshold. To remedy this, a second processing step was taken where a region of interest (ROI) mask crops the image to a trapezoidal shape. The values of the threshold masks and the shape of the ROI mask differed between the two datasets due to different camera orientation and different lighting

conditions. This provided a basic methodology for extraction of lane line pixels.

Data along both routes could not be collected when lane lines were occluded, e.g. by collected snow or leaves. For this reason, lane lines in the camera feed were artificially occluded using further video postprocessing, thereby simulating road coverage conditions. The concept of postprocessing the camera feed in order to simulate different conditions is not entirely novel – Rubaiyat, Qin, and Alemzadeh utilized a similar method in their study in order to analyze resilience of autonomous vehicles to disturbed camera input [30]. The specific postprocessing methodology chosen was to use extracted lane line pixels and draw circles at each, using approximately the same color as the road surface. This resulted in the camera feed now having fully occluding lane lines, making normal detection of lane lines through CV or machine learning techniques impossible. Indeed, if one applies the same lane detection CV technique to detect lane lines on these processed images, no detections would be possible. The result of this CV image processing is shown for the Eaton Proving Grounds test track route in Figure 13, and for the Campus Drive loop route in Figure 14. Lane line geometry extracted from the proxy high-definition map was drawn on top of these images to demonstrate that the methodology is entirely independent of camera-based lane line detections. The occluded lane lines shown in subsequent figures does not perform perfectly, but as this was just for demonstration purposes current results are satisfactory.

Figure 13. Eaton Proving Grounds test track camera frame with lane lines artificially occluded; compare to Figure 8.

Figure 14. Campus Drive camera frame with lane lines artificially occluded; compare to Figure 9.

Metrics of Evaluation

Data Accuracy Metrics

The most important metric for ensuring the quality of collected data was horizontal and vertical accuracy. These metrics are reported by both the Trimble Catalyst DA2 handheld sensor as well as the Swift Navigation Duro Inertial sensor. The Swift Navigation Duro Inertial sensor also operates in several accuracy modes, depending on satellite visibility and mobile network conditions. The highest accuracy mode is RTK fixed, determined by the number of visible satellites and whether the rover is receiving corrections from the base station. The goal of data collection was to keep collected lane line points accurate to 2 centimeters, and to keep the ego vehicle GNSS system operating in RTK fixed mode, accurate to 4 centimeters.

Lane Line Overlay Metrics

At present, no metrics exist for quantitative analysis of projected lane line accuracy. The scope of this study did not include development of such a quantitative metric, instead a qualitative analysis showcasing the current strengths and areas of improvement was selected. Among the hypothesized metrics was quantification of the mean intersection over union over the *drivable region*, that is, the area bounded between the two lane lines. Another metric hypothesized involves using the transformed high-definition map lane line data to construct mathematical equations for the lines on the image, and quantify the geometric distance of detected lane line pixel locations as the error. We highlight the need for exploration and development of a quantitative metric as a topic for future work in the conclusions of this study.

Results

Data Accuracy Analysis

In the lane line data collected with the Trimble Catalyst DA2 sensor over the Campus Drive route, the horizontal accuracy of the collected lane line points never exceeded 2 centimeters, and the vertical accuracy never exceeded 5 centimeters. Weather conditions and mobile network strength were poorer at the Eaton Proving Grounds test track, so despite multiple attempts, the maximum horizontal accuracy reached 7 centimeters, and the maximum vertical accuracy reached 25 centimeters. In general, most collected points had a horizontal accuracy between 1 to 3 centimeters and a vertical accuracy between 6 to 9 centimeters. The lane line data collected along both routes were more than sufficient to create the proxy high-definition map.

The Swift Navigation Duro Inertial sensor consistently operated in the highest accuracy fixed RTK mode for the duration of the Campus Drive route. As such, the Campus Drive route data has very good accuracy; the horizontal accuracy of the ego vehicle GNSS receiver was at most 5.0 centimeters, and the vertical accuracy was at most 7.2 centimeters. The ego vehicle GNSS receiver faced more accuracy challenges at the Eaton Proving Grounds test track, switching from fixed RTK to float RTK mode near the end of the route, when the vehicle was surrounded by trees.

Lane Line Overlay Analysis

Eaton Proving Grounds Test Track

The projected lane lines in the straight road segment of the Eaton Proving Grounds route align very well with the true lane line

locations, and little deviation is observed. This shows the methodology holds promise for determination of occluded lane lines, especially for straight roadways. Two example results from this segment are shown in Figure 15.

(a)

(b)

Figure 15. Two examples of Eaton Proving Grounds camera frames from straight road segments with high-definition map lane line data overlaid on artificially occluded lane lines. These show well-aligned lane lines.

When the ego vehicle entered the more wooded area, the Swift Navigation Duro Inertial sensor switched from the higher-accuracy RTK fixed mode to the lower-accuracy RTK float mode. This resulted in a divergence of the projected lane lines away from the true lane lines. Curves present a challenge to this method, even in RTK fixed mode, as discussed further in the following Campus Drive route results. This divergence is shown in Figure 16.

Figure 16. Eaton Proving Grounds camera frame from a curved road segment with high-definition map lane line data overlaid on artificially occluded lane lines. Deviation from true lane lines occurs in this curved road segment due to the GNSS operating in lower-precision RTK float mode and the insufficient sampling rate of the GNSS heading sensor.

Campus Drive Loop

The transformed and projected lane line geometry aligns well with the lane line pixels in the Campus Drive dataset in straight road segments as well, as shown in two examples in Figure 17. The text overlaid on the images shows the instantaneous Swift Navigation Duro Inertial sensor accuracy and operating mode. Note that the Eaton Proving Grounds dataset did not include this accuracy data due to technical limitations at the time of collection.

(a)

(b)

Figure 17. Two examples of Campus Drive camera frames from straight road segments with high-definition map lane line data overlaid on artificially occluded lane lines. These show well-aligned lane lines.

The largest challenge in this dataset was caused by heading sensor sampling rate and the constantly curving road. As the road curves, any delay in the heading data will cause lateral misalignment of the projected lane lines. This is why IMU data was utilized for corrections, as described in Equation 1. This is shown in Figure 18. These results show that in order to most accurately overlay lane line geometry using high-definition map data, in addition to very high sensor accuracy, the ego vehicle IMU and GNSS sensors must sample at a very high rate, otherwise the projected lane lines will become misaligned with the true lane lines in curves. This problem is less apparent for straight road segments, where the sensed ego vehicle heading does not change much.

Figure 18. Campus Drive camera frame from a curved road segment with high-definition map lane line data overlaid on artificially occluded lane lines. Deviation from true lane lines occurs in this curved road segment due to the insufficient sampling rate of the GNSS heading sensor.

Results Summary

Overall, the results of this proof-of-concept study are encouraging. Lane line geometry was successfully transformed from a proxy high-definition map into a local coordinate frame, then projected onto the camera feed. This allows for the control system of the ego vehicle to utilize high-definition map data in the same way that it would have used camera-detected lane line data, thus solving the problem of lane line occlusion. These results show that this methodology, with sufficient further development, can be used to assist the ego vehicle controller when lane lines become occluded, such as by shadows, leaves, or snow on the road surface.

One challenge with the development of this technology is alignment of the lane lines in curved road segments. Any rotation of the ego vehicle not captured frequently enough will effectively cause a drift of the projected lane lines away from the true lane lines. A very frequently sampled heading sensor could address this challenge. Further development of quantitative metrics is also suggested.

Conclusions

In this paper, we describe and demonstrate a novel methodology to extract lane line geometry through high-definition maps, without the use of real-time camera perception. The lane lines from the high-definition maps were transformed from a global coordinate frame to a local coordinate frame aligned with the camera, and then projected onto the image. This results in the lane lines effectively becoming visible once again and able to be used by the path planning process that would otherwise be inoperable due to lack of input. Overall the results show that this technology concept can be used for augmenting vehicle automation in occluded lane line scenarios. The reconstructed lane lines align very well with the true lane lines in straight road segments, but challenges presently exist with overlay accuracy in curved roads and when GNSS accuracy degrades due to obstruction by trees.

This methodology provides a foundation from which to build an automated navigation procedure robust to lane line occlusion. Perception technology that breaks out of the established norms of camera, radar, and lidar sensing is needed to address the problems of resilient operation and operation in inclement weather. This initial study should be expanded through development of a quantitative measurement in order to rigorously define the accuracy of projected lane lines and enable refinement of the methodology. This could also be compared with artificial intelligence/machine learning based lane line detection algorithms to analyze performance relative to the current state of the art. Furthermore, this methodology can be applied to winter driving, where lane lines may be occluded by snow collected on the road surface and line-of-sight to satellites can be disturbed by cloudy weather or precipitation.

References

1. National Center for Statistics and Analysis, “Traffic Safety Facts 2019: A Compilation of Motor Vehicle Crash Data,” Report No. DOT HS 813 141, US National Highway Traffic Safety Administration, 2021
2. Xu, J., Murphy, S., Arias, E., and Kochanek, K., “Deaths: Final Data for 2019,” Volume 70, Number 8, US Centers for Disease Control and Prevention, 2021, doi:10.15620/cdc:106058
3. National Center for Statistics and Analysis, “Motor Vehicle Traffic Crashes as a Leading Cause of Death in the United States, 2016 and 2017,” Report No. DOT HS 812 927, US National Highway Traffic Safety Administration, 2020
4. US Centers for Disease Control and Prevention, “Web-based Injury Statistics Query and Reporting System (WISQARS) Cost of Injury,” https://wisqars.cdc.gov/cost, accessed Oct. 2022.
5. Insurance Institute for Highway Safety, Highway Loss Data Institute, “Real-world benefits of crash avoidance technologies,” 2020
6. Benson, Tefft, Svancara, et al., “Potential reductions in crashes, injuries, and deaths from large-scale deployment of advanced driver assistance systems,” AAA Foundation for Traffic Safety, 2018
7. Harper, C.D., Hendrickson, C.T., and Samaras, C., “Cost and benefit estimates of partially-automated vehicle collision avoidance technologies,” *Accident Analysis & Prevention* 95(Pt A):104–115, 2016, doi:10.1016/j.aap.2016.06.017
8. Gaikwad, T., Rabinowitz, A., Motallebi Araghi, F., Bradley, T., Asher, Z., Fong, A., and Meyer, R., Vehicle Velocity Prediction Using Artificial Neural Network and Effect of Real World Signals on Prediction Window, *SAE Technical Paper Series*, 2020, doi:10.4271/2020-01-0729
9. Rabinowitz, A., Motallebi Araghi, F., Gaikwad, T., Asher, Z.D., and Bradley, T.H., “Development and Evaluation of Velocity Predictive Optimal Energy Management Strategies in Intelligent and Connected Hybrid Electric Vehicles,” *Energies* 14(18):5713, 2021, doi:10.3390/en14185713
10. Motallebi Araghi, F., Yao, K., Rabinowitz, A., Hoehne, C., Garikapati, V., Holden, J., Wood, E., Chen, S., Asher, Z., and Bradley, T., “Mobility energy productivity evaluation of prediction-based vehicle powertrain control combined with optimal traffic management,” *SAE Technical Paper Series*, SAE International, 400 Commonwealth Drive, Warrendale, PA, United States, 2022, doi:10.4271/2022-01-0141
11. Tunnell, J., Asher, Z.D., Pasricha, S., and Bradley, T.H., “Toward improving vehicle fuel economy with ADAS,” *SAE International Journal of Connected and Automated Vehicles* 1(12-01-02-0005):81–92, 2018
12. Haque, M.R., Islam, M.M., Alam, K.S. et al., “A computer vision based lane detection approach,” *International Journal of Image, Graphics and Signal Processing* 10(3):27, 2019
13. Janai, J., Güney, F., Behl, A. et al., “Computer Vision for Autonomous Vehicles: Problems, Datasets and State of the Art,” *Foundations and Trends in Computer Graphics and Vision* 12(1–3):1–308, 2020, doi:10.1561/0600000079
14. Bounini, F., Gingras, D., Lapointe, V., and Pollart, H., “Autonomous Vehicle and Real Time Road Lanes Detection and Tracking,” *2015 IEEE Vehicle Power and Propulsion*

Conference (VPPC), 1–6, 2015, doi:10.1109/VPPC.2015.7352903
15. US Bureau of Transportation Statistics, "Vehicle Miles Traveled [VMT]," retrieved from FRED, Federal Reserve Bank of St. Louis; https://fred.stlouisfed.org/series/VMT, accessed Oct. 2022.
16. Qiu, L. and Nixon, W.A., "Effects of Adverse Weather on Traffic Crashes: Systematic Review and Meta-Analysis," *Transp. Res. Rec.* 2055(1):139–146, 2008, doi:10.3141/2055-16
17. US Federal Highway Administration, "How Do Weather Events Impact Roads?," https://ops.fhwa.dot.gov/weather/q1_roadimpact.htm, accessed Oct. 2022.
18. Goberville, N.A., Kadav, P., and Asher, Z.D., "Tire Track Identification: A Method for Drivable Region Detection in Conditions of Snow-Occluded Lane Lines," SAE Technical Paper 2022-01-0083, 2022, doi:10.4271/2022-01-0083.
19. Kadav, Parth, Nicholas Goberville, Farhang Motallebi Araghi, Alvis Fong, and Zachary D. Asher. n.d. "Tire Track Identification: Application of U-Net Deep Learning Model for Drivable Region Detection in Snow Occluded Conditions." In *Intelligent Transportation Systems World Congress*.
20. US Federal Highway Administration, "Snow and Ice," https://ops.fhwa.dot.gov/weather/weather_events/snow_ice.htm, accessed Oct. 2022.
21. Shetty, A., Yu, M., Kurzhanskiy, A., Grembek, O., Tavafoghi, H., and Varaiya, P., "Safety challenges for autonomous vehicles in the absence of connectivity," *Transp. Res. Part C: Emerg. Technol.* 128:103133, 2021, doi:10.1016/j.trc.2021.103133
22. Seif, H.G. and Hu, X., "Autonomous Driving in the iCity—HD Maps as a Key Challenge of the Automotive Industry," *Proc. Est. Acad. Sci. Eng.* 2(2):159–162, 2016, doi:10.1016/J.ENG.2016.02.010
23. Poggenhans, F., Salscheider, N.O., and Stiller, C., "Precise Localization in High-Definition Road Maps for Urban Regions," *2018 IEEE/RSJ International Conference on Intelligent Robots and Systems (IROS)*, 2167–2174, 2018, doi:10.1109/IROS.2018.8594414
24. VSI Labs, "Map-based Lane Keeping with HERE HD Live Map," Vision Systems Intelligence, LLC, 2018
25. Trimble DA2 | Catalyst GNSS Systems, https://geospatial.trimble.com/products-and-solutions/trimble-da2, accessed Oct. 2022.
26. Stereolabs, ZED 2i - Industrial AI Stereo Camera, https://www.stereolabs.com/zed-2i/, accessed Oct. 2022.
27. Swift Navigation, Duro Inertial Ruggedized GNSS Receiver Ideal for Outdoor Deployments, https://www.swiftnav.com/duro-inertial, accessed Oct. 2022.
28. Stereolabs, Coordinate Frames, https://www.stereolabs.com/docs/positional-tracking/coordinate-frames/, accessed Oct. 2022.
29. OpenCV Documentation, Camera Calibration and 3D Reconstruction, https://docs.opencv.org/4.6.0/d9/d0c/group__calib3d.html, accessed Oct. 2022.
30. Rubaiyat, A.H.M., Qin, Y., and Alemzadeh, H., "Experimental Resilience Assessment of an Open-Source Driving Agent," *2018 IEEE 23rd Pacific Rim International Symposium on Dependable Computing (PRDC)*, 54–63, 2018, doi:10.1109/PRDC.2018.00016

Contact Information

Kyle Carow
Mechanical & Aerospace Engineering Dept.
Western Michigan University
1903 W Michigan Ave.
Kalamazoo, MI 49008-5314 USA
kyle.j.carow@wmich.edu

Parth Kadav
Mechanical & Aerospace Engineering Dept.
Western Michigan University
1903 W Michigan Ave.
Kalamazoo, MI 49008-5314 USA
parth.kadav@wmich.edu

Johan Fañas Rojas
Mechanical & Aerospace Engineering Dept.
Western Michigan University
1903 W Michigan Ave.
Kalamazoo, MI 49008-5314 USA
johan.fanasrojas@wmich.edu

Zach Asher, Ph.D.
Mechanical & Aerospace Engineering Dept.
Western Michigan University
1903 W Michigan Ave.
Kalamazoo, MI 49008-5314 USA
zach.asher@wmich.edu

Definitions/Abbreviations

CDC	Centers for Disease Control and Prevention
NHTSA	National Highway Traffic Safety Administration
ADS	Automated Driving Systems
AVs	Autonomous Vehicles
ADAS	Advanced Driver Assistance Systems
LDW	lane departure warning
LKA	lane keeping assistance
LCA	lane centering assistance
ODD	operational design domain
CV	computer vision
FHWA	Federal Highway Administration
WMU	Western Michigan University
NED	north, east, down
ROI	region of interest